Editors' Suggestion | Featured in Physics

Loss-Enabled Chirality Inversion in Terahertz Metasurfaces

Weibao He,[1,*] Shun Wan,[1,*] Yunlan Zuo,[2,3] Siyang Hu,[1] Ziheng Ren,[1] Zhongyi Yu,[1] Dongsheng Yang,[4] Xiang'ai Cheng,[1] Keyu Xia,[5,6] Yuze Hu,[4,†] Hui Jing,[4,2,‡] and Tian Jiang[1,4,§]

[1]College of Advanced Interdisciplinary Studies, National University of Defense Technology, Changsha 410073, People's Republic of China

[2]Key Laboratory of Low-Dimensional Quantum Structures and Quantum Control of Ministry of Education, Department of Physics and Synergetic Innovation Center for Quantum Effects and Applications, Hunan Normal University, Changsha 410081, People's Republic of China

[3]School of Physics and Chemistry, Hunan First Normal University, Changsha 410205, People's Republic of China

[4]Institute for Quantum Science and Technology, College of Science, National University of Defense Technology, Changsha 410073, People's Republic of China

[5]College of Engineering and Applied Sciences, Nanjing University, Nanjing 210023, People's Republic of China

[6]Shishan Laboratory, Suzhou Campus of Nanjing University, Suzhou 215000, People's Republic of China

(Received 9 October 2024; revised 11 December 2024; accepted 10 January 2025; published 13 March 2025)

Exceptional points (EPs), known as non-Hermitian degeneracies featuring missing eigenspace dimensions, have led to a variety of intriguing wave phenomena in various physical platforms. Chiral EPs collapsing in two orthogonal eigenstates can lead to unique effects and applications, such as loss-induced transparency, EP-enhanced sensing, and chirality-reversal electronics, etc. However, in previous experiments, chiral EPs were typically induced in fixed structures with inherent active gains or nearby nanotips, which are unfavorable for on-chip integrations with low-power elements. Here, we demonstrate the active control of EPs chirality *in situ* with exceptional-line metasurface. Selective chirality inversion can be well achieved by only light-induced loss without altering the metasurface size. We also perform an ultrafast chirality switch in the picosecond level within transient disturbance. In a broader view, our results provide a platform for the investigation of metasurface-based non-Hermitian physics and active EP modulation, which can stimulate exciting works along this line in near future.

DOI: 10.1103/PhysRevLett.134.106901

Introduction—Recent years have witnessed rapid advances in non-Hermitian physics, featuring exceptional points (EPs) or spectral degeneracies of both eigenvalues and eigenvectors, which have offered chances to build intriguing devices with abilities well beyond conventional Hermitian ones [1–6]. In particular, in optics, EPs have enabled such a wide range of abilities as perfect absorption [7–9], topological phase engineering [10,11], robust entanglement [12,13], enhanced sensing [14–16], unidirectional invisibility [17,18], and anomalous scattering [19], to name only a few. In principle, EPs can be achieved by tailoring the balance of gain and loss [18,20] or tuning the loss imbalance in purely lossy systems [21,22]. However, in practice, random defects or inevitable imperfections of materials can lead to deviations or drifts of the system from the exact positions of EPs, thus radically affecting the performances of the EP devices. Hence, it is highly desirable to make devices with on-site tunability of the EP positions, even allowing flexible switch between distinct EPs in a single device.

Chiral EPs have garnered interest among numerous EP-based studies owing to the connection to natural handedness and its maximally asymmetric behaviors [22–24]. Non-Hermitian metasurfaces, showing flexible control of light unattainable in conventional systems, such as angle-independent focusing [25] or diffraction-order control [26], which can be utilized to enhance their performances in a counterintuitive way [27], provide an efficient platform to study chiral EPs. By tuning the balance of optical loss and coupling strength, chiral EPs can emerge and, thus, enable superchiral fields [24] or spin decoupling modulations [10,28,29]. However, chiral switching or selective chirality inversion, highly required in chiral sensing applications [30], has relied on structural changes [31–33] or an external nanotip perturbing a microcavity [34,35], which suffers from complex operations and lack of flexibility.

Here, we propose and experimentally confirm a scheme to realize an active switch of chiral eigenstates in a terahertz metasurface device. Chiral EP in this case refers to the maximally asymmetric transmission, i.e., either only left- or right-circularly polarized polarization (LCP or RCP,

*These authors contributed equally to this work.
†Contact author: hyz_yj@sina.com
‡Contact author: jinghui73@foxmail.com
§Contact author: tjiang@nudt.edu.cn

respectively). In general, a chiral EP can be created by optimizing two orthogonal coupled modes, which result in fixed circularly polarized vectors as a collapsed eigenstate of the second-order non-Hermitian Hamiltonian. To construct a pair of EPs with opposite chirality in the metasurface, we propose a three-order Hamiltonian from time-domain coupled mode theory (TCMT) and reduce it to a second-order transmission matrix to realize the switch of chiral EPs between two exceptional lines with opposite symbols. Two circular cross-polarized transmission zeros appear at the same frequency, where eigenstates collapse into LCP and right RCP states, revealing the chirality reversal at EPs. We show that the chirality switch can be realized at the ultrafast level of a few picoseconds. No additional gain or structural size changes are required in our device. The missing chiral transmission dimension can be accomplished by only changing the optical pump power. Our work is a timely contribution to such a wide range of fields as non-Hermitian physics, metasurface technology, and terahertz devices, as well as chiral optics and loss engineering.

Switchable chiral EP of Ge-hybrid metasurface—Our metasurface system working at the terahertz regime consists of a metal cut-wire and two split ring resonators (SRRs) embedded with *a*-Ge islands. The *a*-Ge material provides active and tunable dissipative losses for light-driven transmission eigenstates evaluation. To induce chiral EP in non-Hermitian metasurface and switchable chirality inversion, we engineered an asymmetric SRRs with a broken *y*-axis mirror, as shown in Fig. 1(a). The periodicity is set at $P = P_x = P_y = 150$ μm. This mirror-breaking operation will result in two chiral exceptional lines hidden in the metasurface system, which will be discussed as below. To experimentally fabricate the metasurface, we combined UV lithography with stripping processes, as detailed in Supplemental Material (S4) [36]. The resulting metasurface structures were imaged using 20× microscopy, which revealed the precise fabrication of the metastructures [see Fig. 1(b)]. A chiral EP is formed when the incident light causes the two orthogonal eigenstates to collapse into a circular polarization state. Figure 1(c) provides a schematic illustration of the optical pump terahertz metasurface, demonstrating light-driven transmission eigenstates switching. When the metasurface system is operated at low pump power (40 mW), the transmission eigenstates collapse into a left-handed circularly polarized state known as left-handed chiral EP, $|\psi_{\mathrm{EP}}\rangle = (1, -\mathrm{i})^{\mathrm{T}}$. With high-power pumping (270 mW), it can collapse to a right-handed circularly polarized state, $|\psi_{\mathrm{EP}}\rangle = (1, \mathrm{i})^{\mathrm{T}}$, known as right-handed chiral EP. It can be observed that two EPs appear in the parameter space composed of frequency and *a*-Ge conductivity, as shown in Fig. 1(d). The Riemann surfaces of the two eigenvalue magnitudes (red and blue) have two bifurcation points, corresponding to left-handed EP and right-handed EP, respectively. The change in *a*-Ge conductivity induces the metasystem to switch between two EPs at the same frequency.

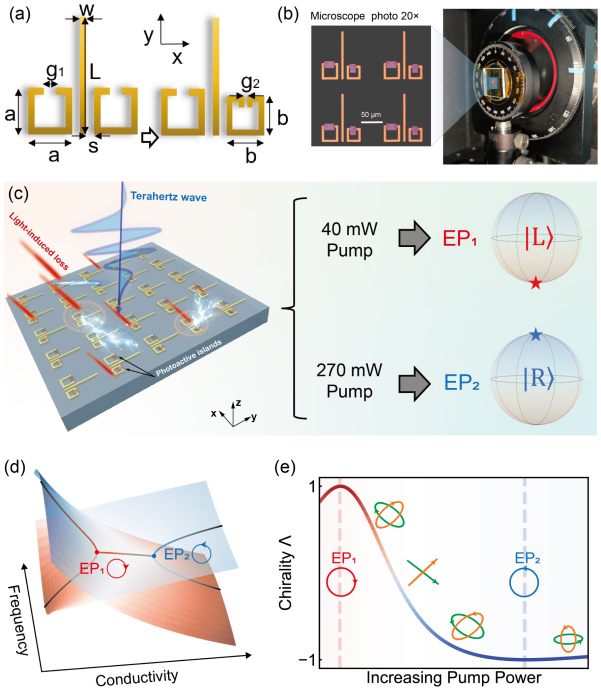

FIG. 1. Light-driven EP chiral inversion in non-Hermitian Ge-hybrid metasurface. (a) Top view of the structural design of the metal metasurface. The lengths are defined as $L = 115$ μm, $a = 39.5$ μm, $g_1 = 15$ μm, $w = 5$ μm, and $s = 8$ μm. To achieve EP chirality inversion, the size of the right SRR is changed to break the *y*-axis mirror symmetry. The parameters are $b = 32.5$ μm and $g_2 = 4$ μm. (b) Non-Hermitian metasurface with microscopic photo under 20× objective lens placed in the optical pump terahertz probe system. It is evident that *a*-Ge islands are embedded in the gap of SRRs. Scale bar, 50 μm. (c) Schematic illustration of the Ge-hybrid metasurface for optical activity. Light excitation increases Ge conductivity, leading to increased system dissipation losses. The system's eigenstate at EP is a left-handed circularly polarized state at a pump power of 40 mW and a right-handed circularly polarized state at 270 mW. (d) The magnitude of the eigenvalues plotted in parameter space of frequency and conductivity. Two EPs appear on the Riemannian surface. (e) Chirality factor varies with increasing pump power. It also illustrates the evolution of eigenstates.

The conductivity of *a*-Ge may affect near-field electric field intensity of SRRs, which further changes the mode dissipation loss [37]. As pump power increases, so does Ge conductivity, resulting in increased system loss. Chirality factor $\Lambda = (|t_{lr}|^2 - |t_{rl}|^2)/(|t_{lr}|^2 + |t_{rl}|^2)$ was defined to characterize the chiral EP state, where t_{rl} (t_{lr}) represents the complex transmittance of RCP (LCP) with LCP (RCP) incident. $\Lambda = 1$ implies a perfectly left-handed circular eigenstate, and $\Lambda = -1$ implies a perfectly right-handed circular eigenstate. Figure 1(e) demonstrates the chirality factor as a function of pump power and illustrates how the chiral EP switches from a left-handed to a right-handed

state as the pump power increases. At specific pump powers, corresponding to the a-Ge conductivities in Fig. 1(e), the eigenstates of metasystem collapse into left- and right-handed circularly polarized states with $\Lambda = 1$ (EP_1) and $\Lambda = -1$ (EP_2), respectively, showing a loss-induced EP chirality inversion. It should be emphasized that, unlike the whispering-gallery-mode (WGM) cavity and the waveguide, which focus on clockwise and counterclockwise in two directions [33,38,39], the metasurface supports all polarization states on the Poincaré sphere, and the chirality is manifested in the asymmetric transmission of circular polarization conversion. In addition, different from the WGM cavity, which can adjust the mode properties using nanotips [34,35], it is quite difficult to realize the active chiral switching of EP in metasurface systems due to the fixed structural parameters. Here, we have used creative design to get around the challenge of active EP and have successfully created an active EP chirality inversion in a non-Hermitian metasurface system for the first time.

Exceptional lines in non-Hermitian metasurface—To explain the active chirality inversion, we have conducted a detailed theoretical analysis here. The investigation of metasurface-based chiral EPs generally starts from the second-order scattering Hamiltonian [10,22]. The relationship between transmission spectra and metasurface Hamiltonian is $T = I - j\gamma_x\gamma_y H^{-1}$. Hence, though the eigenvalues and eigenstates are derived from the transmission spectra, they are still connected to the system's Hamiltonian. We discussed this scenario in Supplemental Material (S1) [36] and discovered that flipping coupling symbols can readily result in EP chiral inversion. However, this method requires structural changes and cannot achieve active EP chiral switching.

An effective solution to address the challenges is to introduce a higher-order non-Hermitian system [40,41]. We further establish a model with three coupled resonant modes, in which two modes can be actively tuned by optical pump, as shown in Fig. S3, Supplemental Material [36], to study the interaction between terahertz pulse and metasurfaces. The metasurface structure corresponding to the theory model consists of one cut-wire and two SRRs, with SRRs located on both sides of the cut-wire to ensure that the coupling symbols between them are opposite.

The TCMT method was used to explain the EPs characteristics of third-order non-Hermitian Hamiltonian with

$$H = \begin{pmatrix} \gamma_{x_2}\gamma_y\Delta\omega_{x_1} + j\gamma_{x_2}\gamma_y X_1 & j\gamma_{x_1}\gamma_{x_2}\gamma_y & \kappa_1\sqrt{\gamma_{x_1}}\gamma_{x_2}\sqrt{\gamma_y} \\ j\gamma_{x_1}\gamma_{x_2}\gamma_y & \gamma_{x_1}\gamma_y\Delta\omega_{x_2} + j\gamma_{x_1}\gamma_y X_2 & \kappa_2\gamma_{x_1}\sqrt{\gamma_{x_2}}\sqrt{\gamma_y} \\ \kappa_1\sqrt{\gamma_{x_1}}\gamma_{x_2}\sqrt{\gamma_y} & \kappa_2\gamma_{x_1}\sqrt{\gamma_{x_2}}\sqrt{\gamma_y} & \gamma_{x_1}\gamma_{x_2}\Delta\omega_y + j\gamma_{x_1}\gamma_{x_2}X_3 \end{pmatrix}, \tag{1}$$

where $\Delta\omega_i = \omega_i - \omega$, $X_i = \gamma_i + \Gamma_i$ $(i = x_1, x_2, y)$, and $j = \sqrt{-1}$. γ is the radiation loss rate, and Γ is the dissipate loss rate. The subscripts represent resonance modes. $\kappa_{1,2}$ quantifies the coupling strength between the resonance modes $a_{x_{1,2}}$ and a_y, respectively. This situation will be different from the second-order Hamiltonian system (for details, see Supplemental Material, S1–S3 [36], which includes Refs. [42–45]). First, consider a structure that is symmetric along the y axis, as seen in Fig. 2(a). Note that we investigate the chiral EP resulting from the coupling of two orthogonal resonance modes along the x and y directions, even though we utilize a third-order Hamiltonian; this is because resonances in different directions can always be decomposed into these two directions. By altering the dissipate loss rates of the two SRR modes, interestingly, two exceptional lines corresponding to the left-handed (red line) and right-handed (blue line) circularly polarized eigenstates, respectively, can be observed in the parameter space of (Γ_1, Γ_2), as shown in Fig. 2(b), while, in practice, the dissipate loss rates of two SRRs will be increased simultaneously with light excitation. Without loss of generality, here we assume that the losses of both SRRs increase linearly under light excitation, marked by black dashed lines. When the radiation loss rates and coupling coefficient with cut-wire of the two SRRs meet the following conditions: $\gamma_1 = \gamma_2$ and $|\kappa_1| = |\kappa_2|$, the eigenstates of the transmission matrix always retain orthogonal linear polarization as the pump power increases as shown in Fig. 2(c). The system in this case is situated on a complex Dirac point [46] as the metasurface structure is entirely symmetrical along the y axis.

To achieve the switching of EP chirality under optical pump at the metasurface, the symmetry of the unit cell needs to be broken down. The specific operation shown in Fig. 2(d) is to meet the condition of $\gamma_1 < \gamma_2$ and $|\kappa_1| < |\kappa_2|$. In practice, we need to adjust the size of one of the SRRs to reduce the radiation loss and coupling coefficient while maintaining the resonance frequency unchanged. As shown in Fig. 2(e), the two exceptional lines intersect successively with the black dashed line, which means the EP chiral switches can be achieved through optical pumping, where the transmission eigenstate of the metasurface system first passes through the left-handed chiral EP and then reaches the right-handed one as pump power increases. We further drew the evolution of the transmission eigenstates along the black dashed line on the Poincaré sphere as shown in

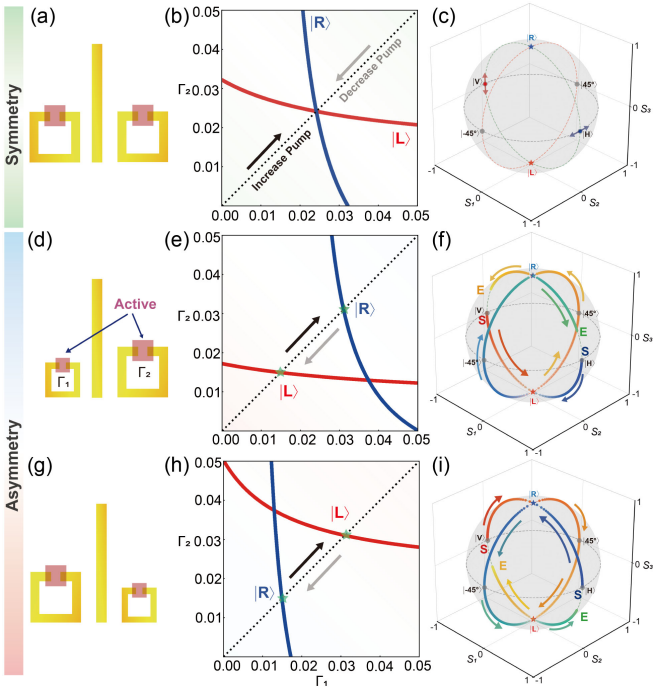

FIG. 2. The actively chiral inversion at EPs in non-Hermitian metasurface consisting of three coupled resonant modes. (a)–(c) In the condition of $\gamma_1 = \gamma_2$ and $|\kappa_1| = |\kappa_2|$, exceptional lines (left-handed circular eigenstate marked by red and right-handed circular eigenstate marked by blue) occur in the parameter space of Γ_1 and Γ_2. The black dashed line denotes that the dissipate losses of two tunable modes increase simultaneously with pump excitation. And the eigenstates always maintain orthogonal linear polarization. (d)–(f) The exceptional lines and the evolution of eigenstates in the condition of $\gamma_1 < \gamma_2$ and $|\kappa_1| < |\kappa_2|$. The eigenstates of non-Hermitian metasurface first degenerate into a left-handed chiral state and then switch to a right-handed chiral state. (g)–(i) In the condition of $\gamma_1 > \gamma_2$ and $|\kappa_1| > |\kappa_2|$, the evolution process is opposite to the former. The colors and arrows along the way indicate the direction of evolution. *S*, start; *E*, end.

Fig. 2(f). As evolution begins, the two eigenstates first collapse to the left-handed circularly polarized state (the Poincaré sphere's South Pole), and then they traverse the entire Poincaré sphere to arrive at the right-handed circularly polarized state (the Poincaré sphere's North Pole). The colors and arrows along the way indicate the direction of evolution.

Likewise, when mirroring the structure along the *y* axis, the exceptional lines exchange the eigenstates and are symmetrical along the black dashed line, as shown in Figs. 2(g)–2(i). The eigenstates undergo a phase transition from left-handed circular polarization to right-handed circular polarization as the pump power increases. By increasing or decreasing the pump, active EP chiral switching can be achieved in the metasurface [indicated by the black arrow in Figs. 2(e) and 2(h)].

Evolution of light-controlled eigenstates—To verify our theoretical design of the EP chiral inversion, we fabricated the non-Hermitian Ge-hybrid metal metasurface consisting of a cut-wire and two SRRs with *a*-Ge islands embedded. Details of the manufacturing process as well as microscopic images and geometric parameters can be found in Figs. 1(a) and 1(b) and Supplemental Material (S4) [36]. To begin with, we utilize numerical simulation to calculate the transmission matrix and eigenstates as a function of *a*-Ge conductivity, as shown in Figs. 3(a)–3(c). The conductivity of the *a*-Ge material we employed, in contrast to steady-state simulation, is based on experimental data from femtosecond laser pump excitation tests. This material has an ultrafast relaxation time of picosecond level [47], which is comparable to the duration of terahertz pulses. For the purpose of modeling and researching the terahertz modulation effect under various *a*-Ge conductivity levels, transient simulation must take care to align terahertz pulses with the relaxation of excited *a*-Ge carriers in time.

It is evident that $|t_{rl}| = 0$ at the parameter of ($\sigma_{\mathrm{Ge}} = 710$ S/m and $f = 0.75$ THz) and $|t_{lr}| = 0$ at the parameter of ($\sigma_{\mathrm{Ge}} = 6700$ S/m and $f = 0.75$ THz) in the terahertz transmission spectra, corresponding to various dissipative losses. The transmission matrix's eigenstates evolve with increasing *a*-Ge conductivity at a frequency of 0.75 THz, initially passing through the Poincaré sphere's South Pole and subsequently the North Pole. At various *a*-Ge conductivities, it exhibits EP chiral inverse, identical to the chiral transmission spectra trend. In order to further confirm this phenomenon, we conducted an experimental demonstration. A method of optical pump terahertz probe is utilized to test the terahertz time-domain transmission spectra of the metasurface under femtosecond pulse excitation (see Supplemental Material, S5 [36]). The data in frequency domain are obtained through fast Fourier

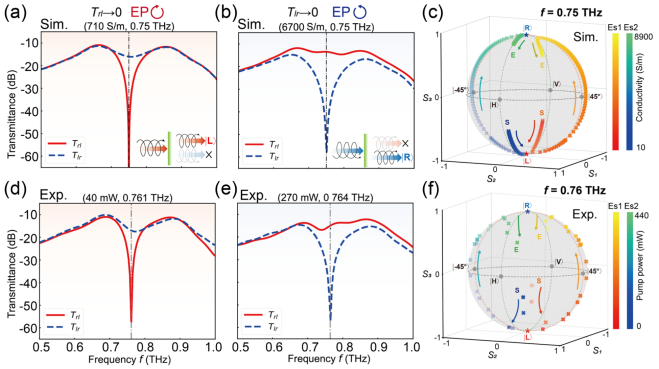

FIG. 3. Light-driven eigenstates evolution for active EP reverse. (a),(b) Numerically simulated chiral transmittance at the position of (710 S/m, 0.75 THz) and (6700 S/m, 0.75 THz). (c) The evolution of eigenstates with *a*-Ge conductivity at a frequency of 0.75 THz. (d),(e) Experimentally extracted chiral transmittance at the positions of (40 mW, 0.761 THz) and (270 mW, 0.764 THz). (f) The evolution of eigenstates with pump power at a frequency of 0.76 THz. Evolution direction of eigenstates with color marker. *S*, start; *E*, end.

transform of time-domain signals. Experimentally extracted chiral transmission spectra are shown in Figs. 3(d) and 3(e). We tested the chiral transmission spectra with various pump powers and found that two different chirality EPs occur at the condition of (40 mW, 0.761 THz) and (270 mW, 0.764 THz), that is, $|t_{rl}| = 0$ for left circular eigenstates and $|t_{lr}| = 0$ for right circular eigenstates.

The EPs were further confirmed by the intersecting double Riemann surface corresponding to the transmission matrix eigenvalues (see Supplemental Material, S6 [36]). It is worth mentioning that, during measuring terahertz time-domain signals, round trips of terahertz pulses occur since the detecting crystal is 1-mm-thick ⟨110⟩ ZnTe (see Supplemental Material, S5 [36]). We so often perform zero-padding analysis after intercepting effective data lengths. As a result, the system's actual true frequency resolution is only around 50 GHz. Therefore, we can be cognizant that two experimental EPs operated at the same frequency, which can be set to 0.76 THz. The experimentally tested eigenstate evolution with various pump powers at 0.76 THz is marked on the Poincaré sphere shown in Fig. 3(f), which is quite close to the simulation findings.

In this manner, we have successfully achieved chiral switching of exceptional points on terahertz metasurface in experiment, operating at a frequency of 0.76 THz. Different from previous studies on flipping spatial structures [31,48] and encircling exceptional points [49,50], our work can reverse the chirality of EP by only increasing or decreasing the pump power. Also, we demonstrate an ultrafast EP chiral inversion under the light pulse excitation within a few picoseconds, providing an indispensable tool for a wide range of applications in chiral optics and ultrafast communications. Figures 4(a) and 4(b) describe experimentally temporal evolution of $|T_{rl}|$ and $|T_{lr}|$, respectively. The spectra extracted at times t_1 and t_2 are shown in Figs. 4(c) and 4(d), respectively, displaying opposite chiral eigenstates within a switching time of 2.7 ps. The spectra extracted at times t_3 and t_4 are shown in Supplemental Material [36]. The illustrations show that the excitation and relaxation of photogenerated carriers in Ge material are responsible for ultrafast switching [47]. The ultrafast modulation process of chiral transmittances and asymmetry factor at 0.76 THz are shown in Figs. 4(e) and 4(f). The type of EP is identified by observing zero crossing chiral transmission as well as the sign of the chiral factor Λ. The simulated data can be found in Supplemental Material [36], which closely matches the experimental results.

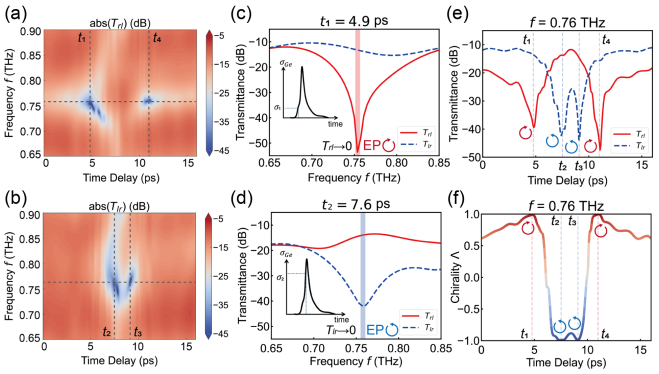

FIG. 4. Experimentally temporal evolution of the chiral transmission in the non-Hermitian metasurface. (a),(b) The chiral spectra of $|T_{rl}|$ and $|T_{lr}|$ as a function of pump probe time delay. The near-zero-transmission magnitude indicated the EP position. (c),(d) Extracted chiral spectra at 4.9 and 7.6 ps. (e),(f) Extracted chiral transmission magnitudes and Λ at 0.76 THz.

Discussion—In conclusion, we have demonstrated a novel approach to achieve active chiral EP inversion in one metasurface, which has not been done in previous metasurface systems. Using TCMT in a three-mode two-port system, we theoretically found two exceptional lines with opposite chirality in the loss parameter space. Through the manipulation of dissipative losses, the chirality of EP can switch between two exceptional lines, that is, active chiral EP inversion. The corresponding metasurface unit proposed in this work consists of a cut-wire and two SRRs embedded *a*-Ge islands at the gaps and works at the terahertz frequency. We can control terahertz-matter interactions by altering the resonance mode dissipative loss resulting from light-induced changes in *a*-Ge conductivity via optically pumped terahertz probe. Here, we investigate the non-Hermitian degeneracy condition supported by a linearly polarized transmission matrix, where two equal eigenvalues appear in the parameter space of frequency and pump power and display the eigenstates of left-handed and right-handed circularly polarized state, respectively. The transient chirality switching process can take only a few picoseconds. Overall, this work shows the potential of controlled bits by providing a metasurface-based EP chirality switching that operates at the same frequency and opens the way for polarization control, holographic multiplexing, and encrypted communication. Our findings may facilitate the study of nonreciprocal phase transitions [51], EP-enhanced phase sensing [52], and EP-based chiral field [53]. Additionally, we can further introduce color-coded metasurfaces to achieve independent control of both SRR modes [54] and will experimentally observe the existence of exceptional lines in the loss parameter space. We believe that the idea of constructing three coupled modes to achieve second-order chiral EP switching can be expanded to include more modes and higher-order non-Hermitian systems. This work demonstrated a versatile and controllable platform for studying the interplay of four important fields of non-Hermitian physics, metasurface, and chiroptics as well as terahertz technology.

Acknowledgments—This work is supported by the National Natural Science Foundation of China (62075240, 62305384, 11935006, and 92365107), the

National Key Research and Development Program of China (2019YFA0308700, 2020YFB2205800, and 2024YFE0102400), the Youth Innovation Talent Incubation Foundation of the National University of Defense Technology (2023-lxy-fhij-007), the Science and Technology Innovation Program of Hunan Province (2020RC4047), Hunan provincial major sci-tech program (2023ZJ1010), and the Program for Innovative Talents and Teams in Jiangsu (JSSCTD202138).

[1] Z. Guo, F. Yang, H. Zhang, X. Wu, Q. Wu, K. Zhu, J. Jiang, H. Jiang, Y. Yang, Y. Li *et al.*, Natl. Sci. Rev. **11**, nwad172 (2024).
[2] C. Wang, Z. Fu, W. Mao, J. Qie, A. D. Stone, and L. Yang, Adv. Opt. Photonics **15**, 442 (2023).
[3] A. Li, H. Wei, M. Cotrufo, W. Chen, S. Mann, X. Ni, B. Xu, J. Chen, J. Wang, S. Fan *et al.*, Nat. Nanotechnol. **18**, 706 (2023).
[4] K. Liao, Y. Zhong, Z. Du, G. Liu, C. Li, X. Wu, C. Deng, C. Lu, X. Wang, C. T. Chan *et al.*, Sci. Adv. **9**, eadf3470 (2023).
[5] Z. Li, C. Li, Z. Xiong, G. Xu, Y. R. Wang, X. Tian, X. Yang, Z. Liu, Q. Zeng, R. Lin *et al.*, Phys. Rev. Lett. **130**, 227201 (2023).
[6] R. Kononchuk, J. Cai, F. Ellis, R. Thevamaran, and T. Kottos, Nature (London) **607**, 697 (2022).
[7] J. Yu, B. Ma, A. Ouyang, P. Ghosh, H. Luo, A. Pattanayak, S. Kaur, M. Qiu, P. Belov, and Q. Li, Optica **8**, 1290 (2021).
[8] W. R. Sweeney, C. W. Hsu, S. Rotter, and A. D. Stone, Phys. Rev. Lett. **122**, 093901 (2019).
[9] C. Wang, W. R. Sweeney, A. D. Stone, and L. Yang, Science **373**, 1261 (2021).
[10] Q. Song, M. Odeh, J. Zúñiga-Pérez, B. Kanté, and P. Genevet, Science **373**, 1133 (2021).
[11] R. Colom, E. Mikheeva, K. Achouri, J. Zuniga-Perez, N. Bonod, O. J. Martin, S. Burger, and P. Genevet, Laser Photonics Rev. **17**, 2200976 (2023).
[12] Z. Tang, T. Chen, X. Tang, and X. Zhang, Light Sci. Appl. **13**, 167 (2024).
[13] Z. Tang, T. Chen, and X. Zhang, Laser Photonics Rev. **18**, 2300794 (2024).
[14] J.-H. Park, A. Ndao, W. Cai, L. Hsu, A. Kodigala, T. Lepetit, Y.-H. Lo, and B. Kanté, Nat. Phys. **16**, 462 (2020).
[15] W. Chen, Ş. Kaya Özdemir, G. Zhao, J. Wiersig, and L. Yang, Nature (London) **548**, 192 (2017).
[16] T. S. Bai, W. Z. Wang, X. Zhang, and T. J. Cui, Adv. Funct. Mater. **34**, 2312170 (2024).
[17] L. Feng, Y.-L. Xu, W. S. Fegadolli, M.-H. Lu, J. E. Oliveira, V. R. Almeida, Y.-F. Chen, and A. Scherer, Nat. Mater. **12**, 108 (2013).
[18] X. Shu, A. Li, G. Hu, J. Wang, A. Alù, and L. Chen, Nat. Commun. **13**, 2123 (2022).
[19] T. He, Z. Zhang, J. Zhu, Y. Shi, Z. Li, H. Wei, Z. Wei, Y. Li, Z. Wang, C.-W. Qiu *et al.*, Light Sci. Appl. **12**, 1 (2023).
[20] H. Hodaei, M.-A. Miri, M. Heinrich, D. N. Christodoulides, and M. Khajavikhan, Science **346**, 975 (2014).
[21] A. Guo, G. J. Salamo, D. Duchesne, R. Morandotti, M. Volatier-Ravat, V. Aimez, G. A. Siviloglou, and D. N. Christodoulides, Phys. Rev. Lett. **103**, 093902 (2009).
[22] M. Lawrence, N. Xu, X. Zhang, L. Cong, J. Han, W. Zhang, and S. Zhang, Phys. Rev. Lett. **113**, 093901 (2014).
[23] Z. Zhou, B. Jia, N. Wang, X. Wang, and Y. Li, Phys. Rev. Lett. **130**, 116101 (2023).
[24] T. Wu, W. Zhang, H. Zhang, S. Hou, G. Chen, R. Liu, C. Lu, J. Li, R. Wang, P. Duan *et al.*, Phys. Rev. Lett. **124**, 083901 (2020).
[25] F. Monticone, C. A. Valagiannopoulos, and A. Alu, Phys. Rev. X **6**, 041018 (2016).
[26] N. S. Nye, A. E. Halawany, C. Markos, M. Khajavikhan, and D. N. Christodoulides, Phys. Rev. Appl. **13**, 064005 (2020).
[27] S. Duan, X. Su, H. Qiu, Y. Jiang, J. Wu, K. Fan, C. Zhang, X. Jia, G. Zhu, L. Kang *et al.*, Nat. Commun. **15**, 1119 (2024).
[28] Z. Yu, W. He, S. Hu, Z. Ren, S. Wan, X. Cheng, Y. Hu, and T. Jiang, Adv. Sci. **11**, 2402615 (2024).
[29] Y. Li, S. Wan, S. Deng, Z. Deng, B. Lv, C. Guan, J. Yang, A. Bogdanov, P. Belov, and J. Shi, Photonics Res. **12**, 534 (2024).
[30] L. Zhang, H.-X. Wang, S. Li, and M. Liu, Chem. Soc. Rev. **49**, 9095 (2020).
[31] Z. Yang, P.-S. Huang, Y.-T. Lin, H. Qin, J. Zúñiga-Pérez, Y. Shi, Z. Wang, X. Cheng, M.-C. Tang, S. Han *et al.*, Nat. Commun. **15**, 232 (2024).
[32] X. Shu, Q. Zhong, K. Hong, O. You, J. Wang, G. Hu, A. Alù, S. Zhang, D. N. Christodoulides, and L. Chen, Light Sci. Appl. **13**, 65 (2024).
[33] A. Li, J. Dong, J. Wang, Z. Cheng, J. S. Ho, D. Zhang, J. Wen, X.-L. Zhang, C. T. Chan, A. Alù *et al.*, Phys. Rev. Lett. **125**, 187403 (2020).
[34] B. Peng, Ş. K. Özdemir, M. Liertzer, W. Chen, J. Kramer, H. Yılmaz, J. Wiersig, S. Rotter, and L. Yang, Proc. Natl. Acad. Sci. U.S.A. **113**, 6845 (2016).
[35] C. Wang, X. Jiang, G. Zhao, M. Zhang, C. W. Hsu, B. Peng, A. D. Stone, L. Jiang, and L. Yang, Nat. Phys. **16**, 334 (2020).
[36] See Supplemental Material at http://link.aps.org/supplemental/10.1103/PhysRevLett.134.106901 for details of theoretical calculations, parameters of the metasurface, details of simulations and experiments, discussions on transmission matrix eigenvalues, and transient EP chiral switching.
[37] J. Gu, R. Singh, X. Liu, X. Zhang, Y. Ma, S. Zhang, S. A. Maier, Z. Tian, A. K. Azad, H.-T. Chen *et al.*, Nat. Commun. **3**, 1151 (2012).
[38] R. Huang, Ş. Özdemir, J.-Q. Liao, F. Minganti, L.-M. Kuang, F. Nori, and H. Jing, Laser Photonics Rev. **16**, 2100430 (2022).
[39] H. Lee, A. Kecebas, F. Wang, L. Chang, S. K. Özdemir, and T. Gu, Elight **3**, 20 (2023).
[40] W. Tang, K. Ding, and G. Ma, Nat. Commun. **14**, 6660 (2023).
[41] Y. Wu, Y. Wang, X. Ye, W. Liu, Z. Niu, C.-K. Duan, Y. Wang, X. Rong, and J. Du, Nat. Nanotechnol. **19**, 160 (2024).
[42] S. Li, X. Zhang, Q. Xu, M. Liu, M. Kang, J. Han, and W. Zhang, Opt. Express **28**, 20083 (2020).

[43] J. A. Fülöp, S. Tzortzakis, and T. Kampfrath, Adv. Opt. Mater. **8**, 1900681 (2019).
[44] S. Fan, W. Suh, and J. D. Joannopoulos, J. Opt. Soc. Am. A **20**, 569 (2003).
[45] T. Dong, S. Li, M. Manjappa, P. Yang, J. Zhou, D. Kong, B. Quan, X. Chen, C. Ouyang, F. Dai, J. Han, C. Ouyang, X. Zhang, J. Li, Y. Li, J. Miao, Y. Li, L. Wang, R. Singh, W. Zhang, and X. Wu, Adv. Funct. Mater. **31**, 2100463 (2021).
[46] P. Pujol-Closa and D. Artigas, Phys. Rev. B **108**, 205106 (2023).
[47] W. X. Lim, M. Manjappa, Y. K. Srivastava, L. Cong, A. Kumar, K. F. MacDonald, and R. Singh, Adv. Mater. **30**, 1705331 (2018).
[48] M. Kang, J. Chen, and . D. Chong, Phys. Rev. A **94**, 033834 (2016).
[49] W. Liu, Y. Zhang, Z. Deng, J. Ye, K. Wang, B. Wang, D. Gao, and P. Lu, Laser Photonics Rev. **16**, 2100675 (2022).
[50] J. Doppler, A. A. Mailybaev, J. Böhm, U. Kuhl, A. Girschik, F. Libisch, T. J. Milburn, P. Rabl, N. Moiseyev, and S. Rotter, Nature (London) **537**, 76 (2016).
[51] M. Fruchart, R. Hanai, P. B. Littlewood, and V. Vitelli, Nature (London) **592**, 363 (2021).
[52] W. Mao, Z. Fu, Y. Li, F. Li, and L. Yang, Sci. Adv. **10**, eadl5037 (2024).
[53] C.-C. Cheng, P.-J. Cheng, T.-W. Huang, W.-T. Wang, J.-T. Tsai, M.-H. Shih, and S.-W. Chang, Optica **10**, 732 (2023).
[54] W. He, X. Cheng, S. Hu, Z. Ren, Z. Yu, S. Wan, Y. Hu, and T. Jiang, Light Sci. Appl. **13**, 142 (2024).